

# An Investigation on the Transition Metal Doping and Energy Band Structure of NaTaO<sub>3</sub> Nanoparticles

Xiaoqing Liu<sup>1</sup>, Yue Meng<sup>2</sup>, and Xiaojing Wang<sup>1+</sup>

<sup>1</sup>Chemistry and Chemical Engineering, Inner Mongolia University, Huhehaote City 010021, China

<sup>2</sup>Inner Mongolia Experiment Research Institute of Geology and Resources, Huhehaote City 010021, China

**Abstract.** M-doped NaTaO<sub>3</sub> (M=V, Cr, Mn Fe, Ni, Cu,Zn) nanoparticles were synthesized by hydrothermal conditions. UV-vis diffuse reflectance spectra clearly indicate the red-shift in the series of M-doped NaTaO<sub>3</sub> catalysts, resulting in a different decrease in the band gap of NaTaO<sub>3</sub> caused by the different doping element. The structure of the energy band was obtained by density functional theory. The substitution of Ta<sup>5+</sup> by metal ions results in forming an intermediate band (IB), which is mainly attributed to the state of metal 3d. It not only decrease the band gap but also increase the transient behavior of the photogenerated charge carriers and inhibit the recombination of e<sup>-</sup>-h<sup>+</sup> pairs, showing enhanced photo-absorbed and photocatalytic activities over the entire visible region.

**Keywords:** Metal doped NaTaO<sub>3</sub>, Hydrothermal, Photocatalyst, Energy band Density functional theory

## 1. Introduction

Exploitation of new energy sources has gained considerable attention due to the worldwide energy shortage and environment pollution. The development of efficient visible-light-driven semiconducting materials is a vital requirement for the photocatalytic splitting of water to produce hydrogen and for the photooxidation of organic compounds causing pollution in order to effective harnessing of solar energy [1-2]. In recent years, perovskite-type alkali tantalates, ATaO<sub>3</sub> (A = Li, Na, and K) show reasonable activities for water splitting under UV irradiation. However, the alkali tantalates are usually less active under visible-light irradiation [3-4]. The transition metal ions, was found to be attractive dopant for the effective modification of photocatalysts, which can play multiple roles ranging from decrease in band gap to efficient transfer of electron due to its multiple oxidation states [5-6]. Electron transitions from the valence band to the dopant level or from the dopant level to the conduction band can effectively red shift the band edge absorption threshold. This research is aimed to investigate the doping effect of metal ions on the energy band structure and the response to the visible light. The uniformly and highly dispersed state of the metal ions incorporated tantalate was prepared. The role of metal ions in promoting the response to the visible light was well followed and investigated by exploring the atomic occupation of metal dopant and the electronic structures using the density functional theory (DFT).

## 2. Details of experiment and calculation

M-doped NaTaO<sub>3</sub> nanoparticles were prepared by by hydrothermal method. Mixture of Ta<sub>2</sub>O<sub>5</sub> and metal oxide was ground well in an agate mortar in molar ratio of 1:0.25, 1:0.50, 1:0.75, 1:1 and 1:1.25, respectively. This mixture was added into a Teflon-lined autoclave of 30 mL together with 45g NaOH with magnetic stirring. Then, the autoclave was sealed and maintained at 200°C for 24h. After cooling to room temperature in air naturally, the mixture was filtered and washed with distilled water, and then dried in air at 60°C for 12h.

---

<sup>+</sup> Corresponding author. Tel.: +86-471-4994406; fax: +86-4714992981.  
E-mail address: wang\_xiao\_jing@hotmail.com.

A series of crystalline white powder of M- doped  $\text{NaTaO}_3$  products were obtained. The products were denoted according as the adding metalelement as V-doped  $\text{NaTaO}_3$ , Cr-doped  $\text{NaTaO}_3$ , Mn-doped  $\text{NaTaO}_3$ , Fe-doped  $\text{NaTaO}_3$ , Ni-doped  $\text{NaTaO}_3$ , Cu-doped  $\text{NaTaO}_3$ , and Zn-doped  $\text{NaTaO}_3$ . The properties and the crystalline structure of the materials were studied by using X-ray powder diffraction (XRD), STEM, UV–vis techniques. The electron and energy band structure of  $\text{NaTaO}_3$  and M-doped  $\text{NaTaO}_3$  crystals were calculated on the basis of the density functional theory. The  $2 \times 2 \times 2$  supercell of the 40-atom models was constructed for non-doped  $\text{NaTaO}_3$  and metal doped  $\text{NaTaO}_3$  by substituting a metal atom for Ta atom (Figure 1). The total density of states (TDOS) and the projected density of states (PDOS) for non-doped  $\text{NaTaO}_3$  and each optimized M-doped  $\text{NaTaO}_3$  structure was calculated using the tetrahedron method with Blochl corrections.

### 3. Results and discussion

The prepared specimen was characters by XRD. The diffraction peaks of all the samples can be readily indexed as a pure orthorhombic phase of  $\text{NaTaO}_3$ , identical to the reported standard diffraction data in JCPDS cards (73-0878) (Fig. 1). No characteristic peak of metal oxides were found in the XRD patterns implying either metal ions was incorporated in the crystalline of  $\text{NaTaO}_3$ , or metal oxide was very small and highly dispersed. Broad XRD peaks indicate the formation of nanosized  $\text{NaTaO}_3$  particles. It appears that the metal ions doping did not result in significant structural changes for  $\text{NaTaO}_3$ . However, when the enlarging the (020) peak of the M-doped samples in Figure 2 (Cr ion doping as an example), a systematic shift of the diffraction peaks toward bigger angles was observed, confirming that at least a part of Cr are doped into the crystal lattice of  $\text{NaTaO}_3$ . The angle shift may be attributed to the difference in the ionic radius: The radius of the  $\text{Cr}^{3+}$  ions is 0.061 nm, which is smaller than that of 0.078 nm for  $\text{Ta}^{5+}$  ions [7]. Whereas for the sample of Cu ions doping, the small angles shift of the (020) diffraction peaks was observed due to the large radius of  $\text{Cu}^{2+}$ . Actually in our experiment, the directions of the diffraction angle shift are consistent with their radius, indicating an expended or contractive cubic cell volume.

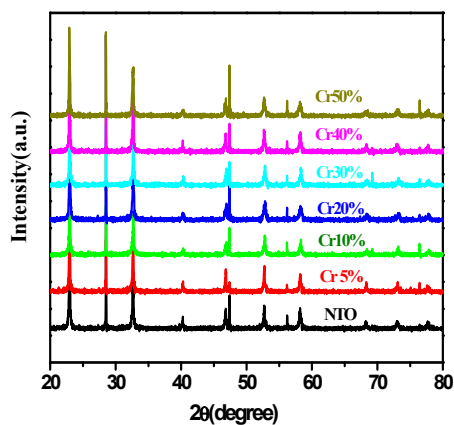


Fig.1 XRD patterns of Cr-doped  $\text{NaTaO}_3$ .

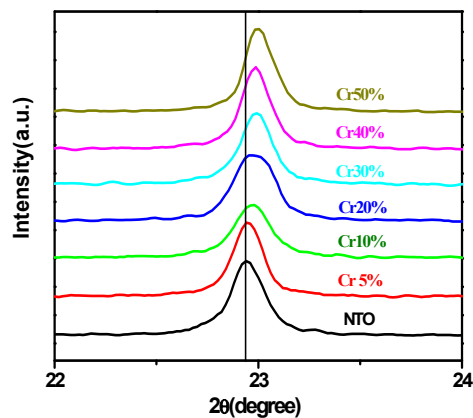


Fig. 2: The (020) peak of Cr-doped  $\text{NaTaO}_3$ .

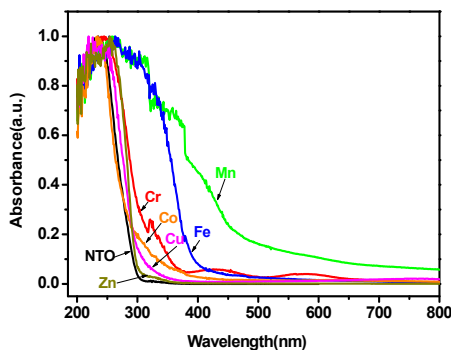


Fig. 3: Diffuse reflectance spectrum of  $\text{NaTaO}_3$  doped with metal ions.

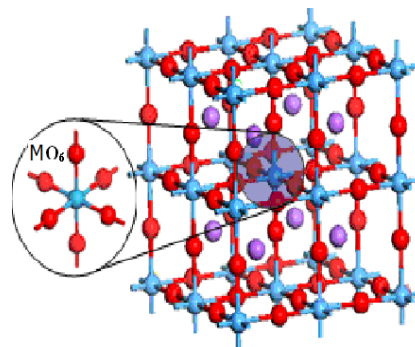


Fig. 4: Supercell of M-doped  $\text{NaTaO}_3$   $2 \times 2 \times 2$  (40-atoms).

Optical diffuse reflectance spectra of both undoped and M-doped NaTaO<sub>3</sub> nanoparticles, measured at room temperature are shown in Figure 3. The undoped NaTaO<sub>3</sub> shows a absorption at 300 nm, indicating the band gap energy of 4.13 eV. Compared with the spectrum of pure tantalates, the red-shift was clearly observed in the series of the different metal doped NaTaO<sub>3</sub> catalysts. The effect becomes more prominent with increasing metal ions concentration, indicating a decrease in the band gap of NaTaO<sub>3</sub> caused by substitution of the different metal ions at tantalum site.

The DFT calculation in this work was carried out using CASTEP code. The supercell structure is shown in Figure 4. The optimized lattice parameters are  $a=b=c=8.085$  for non-doped NaTaO<sub>3</sub>, which are in good agreement with the experimental results [9], indicating that our methodology is reasonable. To study the doping effect, a Ta atom was substituted by an metal atom in each 2×2×2 super cell (40 atoms), giving a doping level of 1/16 of the Ta lattice sites. The total density of states (TDOS) and projected density of states (PDOS) of the pure NaTaO<sub>3</sub> and vanadium doped NaTaO<sub>3</sub> were calculated (Fig. 5). Figure 6 shows the energy band structure of pure NaTaO<sub>3</sub> and M-doped NaTaO<sub>3</sub>. As illustrated in Figure 5 and 6, the bandgap for NaTaO<sub>3</sub> is 1.76 eV, which is consistent with the reported results [8]. This band gap is underestimated when compared with that of 4.0 eV for tatanate experimentally observed, which is popular when using DFT simulation. The valance band originates from the fully filled O2p bonding state, while the conduction band results from the Ta5d nonbonding state in the TaO<sub>6</sub> octahedra arranged in the periodic crystal lattice for pure NaTaO<sub>3</sub>. The conduct band (CB) of M-doped NaTaO<sub>3</sub> is dominated by the Ta 5d states and the valence band (VB) is mainly due to occupied O 2p states (Fig. 5). An intermediate band (IB) is clearly observed below the conduct band (CB) in M-doped NaTaO<sub>3</sub>. The IB is attributed to the t<sub>2g</sub> level, mainly composite of the state of M(3d) (Fig. 6). Meanwhile the broadening of valence band was observed which is dictated by the hybridization between the M 3d and O 2p states (Fig. 7). The electronic transitions from the valence band to dopant level or from the dopant level to the conduction band can effectively red shift the band edge absorption threshold. A big dispersion of valence band implies the photoexcited holes could be well delocalized, so that it is favorable to be transferred to the surface. Accordingly, the solar energy conversion efficiency is expected to increase when compared to that of non-doped NaTaO<sub>3</sub>.

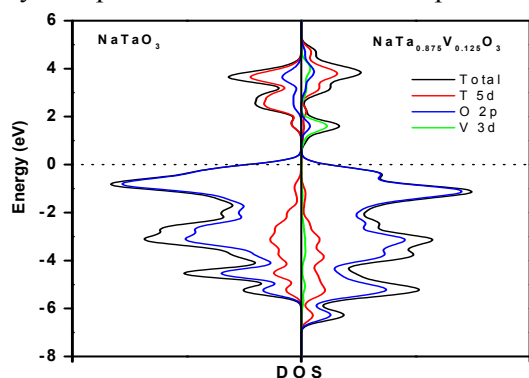


Fig. 5: Total density of states and projected density of states of the pure and V-doped NaTaO<sub>3</sub>

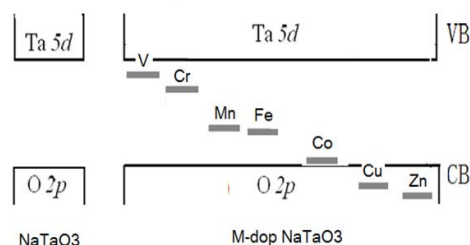


Fig. 6. The intermediate band forming by the d orbital of the doping metal ions

## 4. Conclusions

In summary, well-crystallized NaTaO<sub>3</sub> and M-doped NaTaO<sub>3</sub> nanoparticles were synthesized by a facile hydrothermal method. XRD results shows no significant variations in the size, crystallinity, and crystal structure for M-doped NaTaO<sub>3</sub>, compared to the undoped NaTaO<sub>3</sub>, confirming the formation of pure NaTaO<sub>3</sub> in all samples. The modification of metal ion in NaTaO<sub>3</sub> causes a red-shift in the UV-Vis spectra, implying the capability of controlling on the band gap by metal doping. The presence of metal ions in tantalates introduces new energy levels into the band gap of NaTaO<sub>3</sub>, which results in the red shift of the absorption spectra. The electronic transitions from the valence band to dopant level or from the dopant level to the conduction band can effectively red shift the band edge absorption threshold. The response to the visible light was improved by the intermediate band formed by the d orbital of doping metal ions.

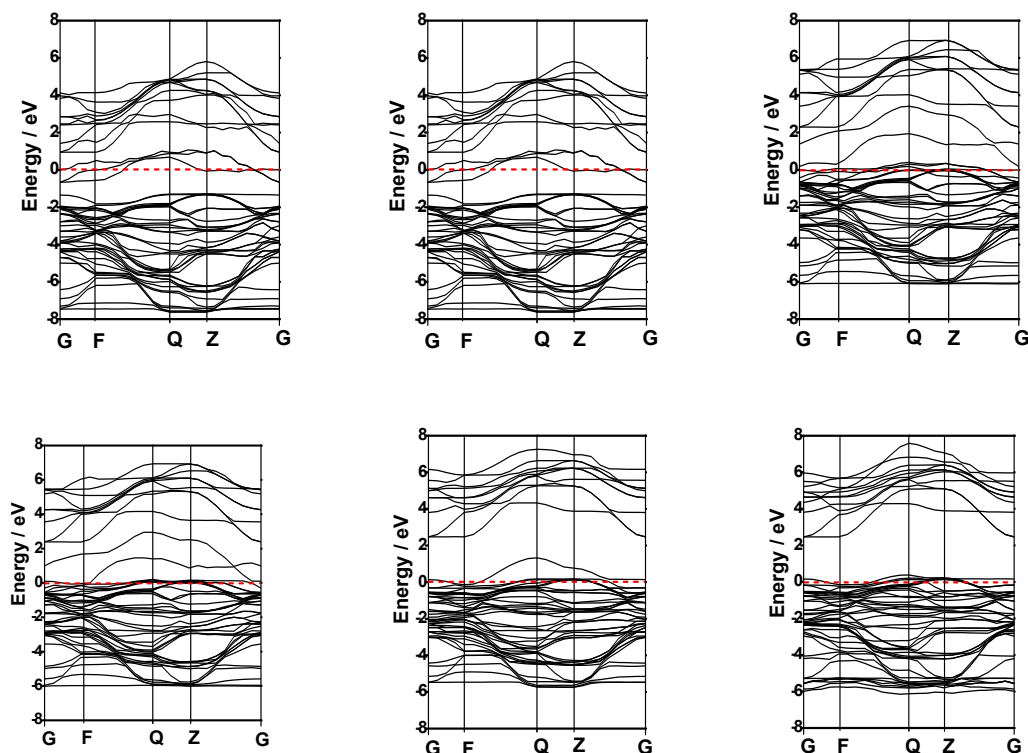


Fig.7 M-doped NaTaO<sub>3</sub> in the first Brillouin Zone, (a), (b), (c), (d), (e), and (f) are Cr<sup>3+</sup>, Mn<sup>2+</sup>, Fe<sup>3+</sup>, Co<sup>2+</sup>, Cu<sup>2+</sup>, Zn<sup>2+</sup>-doped NaTaO<sub>3</sub>, respectively

## 5. Acknowledgment.

This work is supported by the National Natural Science Foundation of China (Nos. 20967004), the inner Mongolia National Science Foundation (2010Zd08), the Project of Scientific and Technological Innovation Team of Inner Mongolia University (12110614).

## 6. References

- [1] A. Kudo, R. Niishiro, A. Iwase, H. Kato. Effects of doping of metal cations on morphology, activity, and visible light response of photocatalysts. *Chem. Phys.* 2007, **339**: 104–110.
- [2] J.F. Zhu, M. Zäch, Nanostructured materials for photocatalytic hydrogen production. *curr. opin. colloid interface sci.* 2009, **14**: 260–269.
- [3] C. Zhou, G. Chen, Y.X. Li, H.J. Zhang, J. Pei, Photocatalytic activities of Sr<sub>2</sub>Ta<sub>2</sub>O<sub>7</sub> nanosheets synthesized by a hydrothermal method. *Int. J. Hydrogen Energ.* 2009, **34**: 2113–212.
- [4] R. Shi, J. Lin, Y.J. Wang, J. Xu, Y.F. Zhu, Visible-Light Photocatalytic degradation of BiTaO<sub>4</sub> photocatalyst and mechanism of photocorrosion suppression. *J. Phys. Chem. C* 2010, **114**: 6472–6477.
- [5] D.W. Hwang, H.G. Kim, J.S. Lee, J. Kim, W. Li, S. H. Oh, Photocatalytic hydrogen production from water over M-doped La<sub>2</sub>Ti<sub>2</sub>O<sub>7</sub> (M =Cr, Fe) under visible light irradiation ( $\lambda > 420$  nm). *J. Phys. Chem. B* 2005, **109**: 2093–2102.
- [6] C. Diaz-Guerra, P. Umek, A. Gloter J. Piqueras, Synthesis and cathodoluminescence of undoped and Cr<sup>3+</sup>-doped sodium titanate nanotubes and nanoribbons. *J. Phys. Chem. C* 2010, **114**: 8192–8198.
- [7] A. Kleiman-Shwarscstein, Y.S. Hu, A.J. Forman, G.D. Stucky, E.W. McFarland Electrodeposition of  $\gamma$ -Fe<sub>2</sub>O<sub>3</sub> doped with Mo or Cr as photoanodes for photocatalytic water splitting. *J. Phys. Chem. C* 2008, **112**: 15900–15907.
- [8] X. Wang, H. Bai, Y. Meng, Y. Zhao, C. Tang, and Y. Gao, Synthesis and optical properties of Bi<sup>3+</sup> doped NaTaO<sub>3</sub> nano-size photocatalysts. *J. Nanosci. Nanotech.* 2010, **10**: 1788–1793.